One-pot mechanochemical synthesis of Cu and Pt-doped MnO_x nanostructures as efficient catalysts in CO_2 hydrogenation reaction; Manganase-balance drives activity

Altantuya Ochirkhuyag[a], András Sápi[ab], Ákos Kukovecz[ac], Zoltán Kónya[ac*]

[a] *University of Szeged, Interdisciplinary Excellence Centre, Department of Applied and Environmental Chemistry, H-6720, Rerrich Béla tér 1, Szeged, Hungary*

[b] *Institute of Environmental and Technological Sciences, University of Szeged, H-6720, Szeged, Hungary*

[b] *MTA-SZTE Reaction Kinetics and Surface Chemistry Research Group, University of Szeged, H-6720 Szeged, Rerrich Béla tér 1, Szeged, Hungary*

**corresponding authors: wizipisztoly@gmail.com*

Abstract

Here we report a novel mechanochemical synthesis of manganese oxide nanoflakes and nanorods. As synthesized pure oxides and metal (Pt and Cu) doped oxides all tested in the CO2 hydrogenation reaction. Our study demonstrates a successful synthesis of the manganese oxide nanoparticles by mechano-chemical synthesis. It is revealed that the milling speed can tune the crystal structure and oxidation states of the manganese (+2, +3 and +4), which plays an important role for the CO2 hydrogenation. The pure MnOx milled at 600 rpm showed similarly high catalytic activity (~20.000 nmol*g–1*s–1) as Pt-loaded and Cu-loaded counterparts showing the important role of the structure of the manganese-oxide under reaction conditions. However, the Pt-loading boosted the methane's selectivity showing the influence of the Pt/MnOx interface. It is compromised that milling method is a useful method for the production of highly active pure and doped manganese nanoparticle by cost-effective simple way.

Keywords: manganese oxide, nanoparticle, milling, hydrogenation, catalyst

1. Introduction

All over the world, we have considerable problems mainly from the environmental pollutions, global warming, extreme weather changes caused by the emission of CO_2 and more energy consumption than producing energy from a conventional energy source such as fossil fuel burning. Due to decreases of non-renewable energy source and global environmental problem of greenhouse gas (including CO_2), suitable energy production development is becoming one of the most crucial tasks. For that reason, CO_2 hydrogenation is a promising candidate for the next-generation energy production challenge on account of the environmental good impact and cost-effective property[1,2].

But CO_2 hydrogenation process is an endothermic slow process and efficient catalysts are necessary for the reaction. Metal-based, heterogeneous catalysts such as Cu/ZnO, Cu/SiO_2, Ni/CeO_2 and homogeneous catalysts $RhCl(PPh_3)_2(Net_3)$ are the most studied CO_2 hydrogenation catalysts[3]. But manganese is would be a good candidate for the cost-efficient catalyst for CO_2 hydrogenation reaction due to abundance in the earth crust and sea nodules as a minerals pyrolusite, braunite, birnessite and cryptomelane distributed all over the world[4,5]. Manganese compounds have a crucial role for the living organism in soil, aqua-system and essential nutrient for human metabolism[6]. Except for this biological importance, manganese oxide-based materials are a promising candidate for the supercapacitor, the electrochemical cell for a rechargeable battery, degradation of organic dyes, removal of the heavy metals from the polluted water, water oxidation catalysts and catalyst for soot combustion[7–13]. Moreover, manganese oxides are showing promising catalytic activity for the CO_2 hydrogen process in the literatures[14].

However, various type of manganese oxides synthesis is going on a laboratory scale perfectly, it has a drawback for the industrial level in real life. Therefore, the mechanochemical synthesis method is suitable for a larger amount of production in real life, not necessarily follow strict control for all synthesis condition as like chemical synthesis and easy to control mean parameters of the milling process. Mechanical milling and mechanochemical synthesis are producing a variety of nanomaterials[15] including various type of manganese oxides[16–19].

Here we report a simple and cost-effective, mechanochemical, one-pot synthesis method to produce pure, Pt-loaded as well as Cu-loaded birnessite type manganese oxide nanoflakes for the first time. Also, we show that these materials are promising candidates for using them in catalytic CO_2 hydrogenation. In this study, the mechanical milling is improved with the crucial factor of synthesis by the chemical redox reaction takes place between Mn^{7+} and Mn^{2+} resulted in colourful $Mn^{4+}/Mn^{3+}/Mn^{2+}$ ion-containing mixed oxides playing an important role in effective catalytic CO_2 hydrogenation.

2. Result and discussion

2.1. Structural determination and chemical characterization

X-ray diffraction patterns of the milled samples showed in **Fig 1a.** The main reflection peaks at 12.4°, 25.1°, 36.9° and 65.4° of the sample milled at 200 rpm (M200) is correlated with birnessite type σ-MnO_2 (JCPDS 421317)[20,21] and peak at 18.8° reveals amorphous Mn_3O_4 phase. The reflection peaks at 12.4°, 25.3°, 36.5°, 44.6° and 65.4° of the sample milled 450 rpm (M450) is related to the mixed-phase of the birnessite type σ-MnO_2 (JCPDS 421317)[22] and hausmannite type Mn_3O_4 (JCPDS 011127)[23]. For the sample 600 rpm (M600) milled showed only 3 major reflection peaks at 36.2°, 44.6° and 64.6° those are matching with amorphous Mn_3O_4 (JCPDS 011127)[23,24]. Owing to increases of milling speed, kinetic energy and temperature are increased inside of the milling chamber and interlayer separating water molecule amount decreases causing to weakening the layered structure of the birnessite. Additionally, manganese (IV) oxide could be reduced to manganese (III and II) oxides such as M450 and M600 samples in alkaline condition. Metal (Pt and Cu) doped sample results prevailed in Supplementary Material **Fig S1.** and there are no more additional peaks from the dopant which is illustrating that dopant amount is not distracting the original crystal structure of the manganese oxides.

Raman *spectra* of the samples are revealed in **Fig 1b** and the characteristic Raman shifts at 641cm^{-1} assigned to the Mn–O symmetric stretching vibration for all three manganese oxides. The shift at 575 cm^{-1} is representing Mn-O symmetric stretching vibration in the basal plane of [MnO_6] sheets of birnessite and is dependent on the presence of Mn^{4+} ions in sample M200 and M450, respectively[25]. In the case of M600, Raman shift at 575 cm^{-1} is disappeared due to oxidation state changes Mn^{3+} and Mn^{2+} ion increases in the structure which is caused to changes from layered manganese (IV) structure to the amorphous hausmannite type manganese (III) oxide[26]. Raman shifts of the metal-doped samples are presented in Supplementary Material **Fig S2** and Raman shifts' position is almost similar to pure samples and only intensities of the shift have declined.

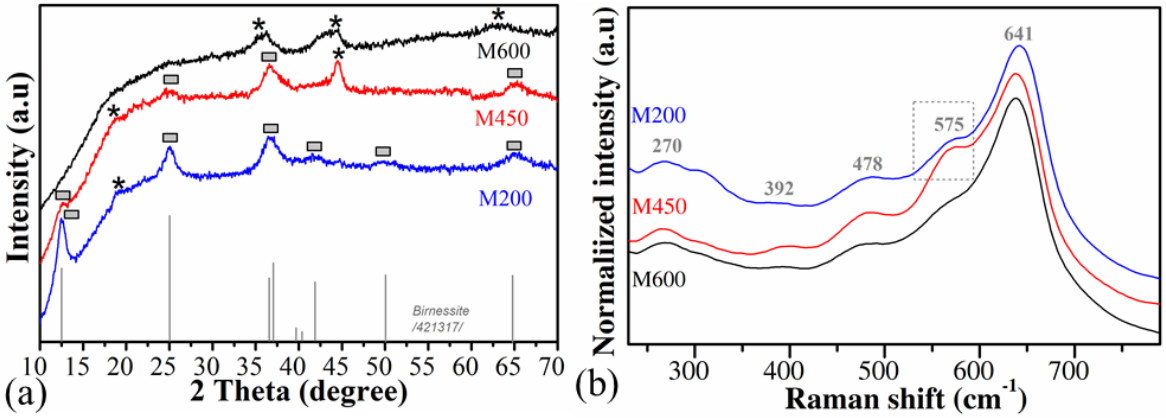

Figure 1. X-ray diffraction patterns of the milled samples (a) {* *birnessite type σ-MnO_2*, ■ *Mn_3O_4 phase*}and Raman spectra of samples (b).

Energy-dispersive X-ray spectroscopic spectra showed in **Fig S3** and quantitative analysis result revealed in **Table S1**. The atomic ratio (molar) of the manganese and oxygen is around 1:2 and the atomic ratio of the manganese and sodium are around 1:0.3[27]. In the case of platinum and copper doped samples, the atomic ratio of manganese and metal (Pt or Cu) is around 1:0.02[28]. If consider weight percentage, Pt and Cu have less than 3% of the composition. However, oxygen, manganese, potassium, sodium and doped metal elements are the main continents, there is a minor amount of impurities would be existing such as iron from the milling bowl.

2.2. Morphological characterization

The specific surface area measurement result showed in **Fig 2a**. Depends on milling speed, the surface area of the sample is increased from 11 m^2/g to 150 m^2/g for M200 and both M450, M600, respectively presented in **Table 1**. Pore radius of the M200 sample is less than 2 nm microporous nevertheless M450 and M600 samples have pores with radius more than 6 nm and presented mesoporous property in **Fig S4**. Milled samples have a relatively high specific surface area than average manganese oxides nanoparticles in the literature[29,30].

Table 1. Specific surface area results of the samples

Samples	Specific surface area m^2/g	Pore radius, nm	Pore volume, cc/g
M200	11	<2	0.06
M450	159	>5.7	0.7
M600	159	>5.8	0.6

Thermogravimetric analysis results of the samples are shown in the **Fig 2b**. Thermal decomposition steps are similar to typical synthetic birnessites for the sample M200 and M450. *First* decomposition step illustrated for M200 and M450 weight losses about 6 percentages both that is revealed a release of physically adsorbed water until 110°C[31]. *Second* weight change for M200 weight losses about 2 percentages at 220 °C owing to releases of physically sorbed water from the interlayer as like typical birnessite sample in the literature[32]. *The third* weight loss occurred at 500 °C for M200 which corresponds reduction of Mn(+4) to Mn(+3) formation of Mn_2O_3[33]. The sample M450 shows similar weight losses about 1.5 % at 570 °C corresponds to the reduction of Mn(+3) to Mn(+2, +3) formation of Mn_3O_4. *Fourth* change around 1% of the weight is gained at 500 °C which corresponds oxidation of manganese for the formation of **α-MnO_2** for M200[34]. Moreover, the *fourth* change of M450 sample occurred at 570°C which is correlated oxidation of manganese for the formation of **α-MnO_2** also possible that formation of **Mn_2O_3**[34,35]. *The fifth* change is occurred for M200 samples due to the rest of Mn_2O_3 reduced to **Mn_3O_4** at 680°C[36]. However, thermal decomposition occurs quite differently for the M600 sample due to manganese oxidation state difference and there totally 3 changes revealed. The *first* decomposition occurs at 110 °C about 4% of weight which is physically adsorbed water releases. The *second* change around 1% of weight gain at 200 °C that is owing to the oxidation of manganese phase change Mn_3O_4 to Mn_2O_3[34]. *Third* change about 2% of weight loss appeared due to the reduction of Mn_2O_3 to Mn_3O_4[36]. Oxidation occurs easily at a lower temperature for the M600 sample indicates that the amount of Mn(+3) is quite higher than the other two samples, it also illustrates weak crystallization of the amorphous morphology[31]. Thermogravimetric analysis repeated in nitrogen flow and the disclosed in **Fig S5 (a-d)**. In nitrogen flow measurement no weight gain occurred at 300 °C - 550 °C for the M600 sample which is a compromise that oxidation occurs when air is flowing into the system as shown in Fig 2b. X-ray diffraction patterns of the sample after TG analysis is displayed in **Fig S6 (a-b)** and diffraction patterns matched up with **α-MnO_2** and **Mn_2O_3** left after a thermal decomposition for M200. In the case of M450, **α-MnO_2** and Mn_3O_4 phase formed. As a tribute to M600, only Mn_3O_4 is formed. From the thermal gravimetric analysis, the oxidation state ratio of manganese could be suspected such as M200 is mainly consisted of MnO_2 (manganese oxidation state: +4), and M450 consists of MnO_2 and a minor amount of Mn_3O_4 (manganese oxidation state: less than +4, higher than +2 and +3) and M600 consists of almost pure phase Mn_3O_4 (manganese oxidation state: less than +3, higher than +2).

Differential scanning calorimetric results presented in **Fig S5e**. First strong endothermic peaks observed for M200 and M450 related to the dehydration of interlayer water and formation of Mn_2O_3. The second endothermic peak illustrates that reduction of manganese (III) and phase

transition to tunnel structured rod-like Mn_3O_4[37]. In the case of M600, also 2 endothermic peaks observed but peak intensity is weaker than two other samples. First weak corresponds to the physically sorbed water releases and the second peak illustrates a crystallization of rod-like Mn_3O_4.

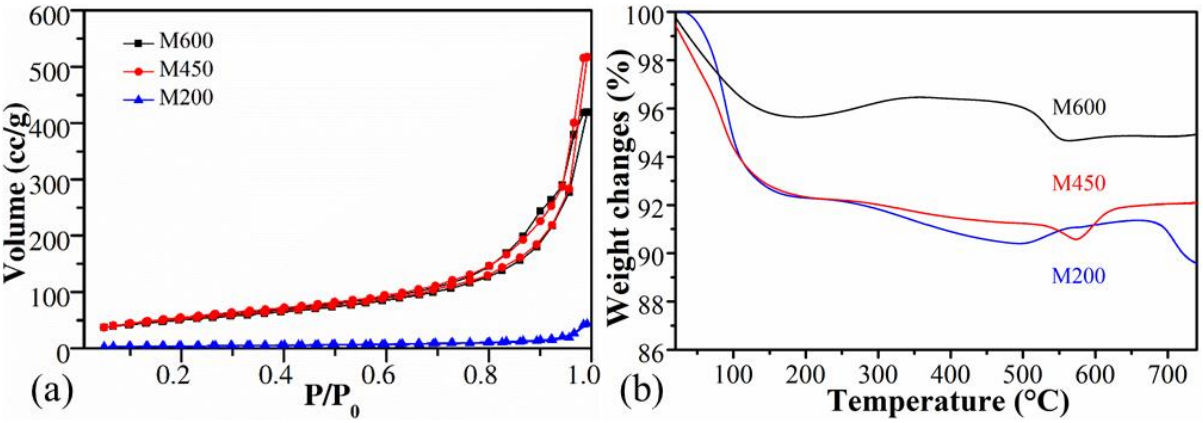

Figure 2. N_2 adsorption analysis full isotherm (a) and thermal decomposition of the samples a heating rate of 5 ◦C min−1 in the air (b).

Scanning electron microscopic *(SEM)* and high-resolution ***transmission electron microscopic*** (HR-TEM) images showed in **Fig 3 (a-c)** and **(d-f)**, respectively. Average particle size is decreased as a consequence of increases in milling speed. M200 sample has larger flake like aggregated sheets identical to the typical birnessite[17] and crystallization is higher than the other two samples. According to milling speed increases, the temperature has increased inside of the milling bowl which is affecting to the decreases of interlayer water which works as the function of the separator of the interlayer in the crystal structure. Further, more reduction takes place and an average oxidation state of manganese for the final product is decreased in case of M450 and M600 series samples. M450 consisted of a mixture of sheet-like flakes and rod-like particles. M600 consists mostly of 10-50 nm small rod-like particles[38].

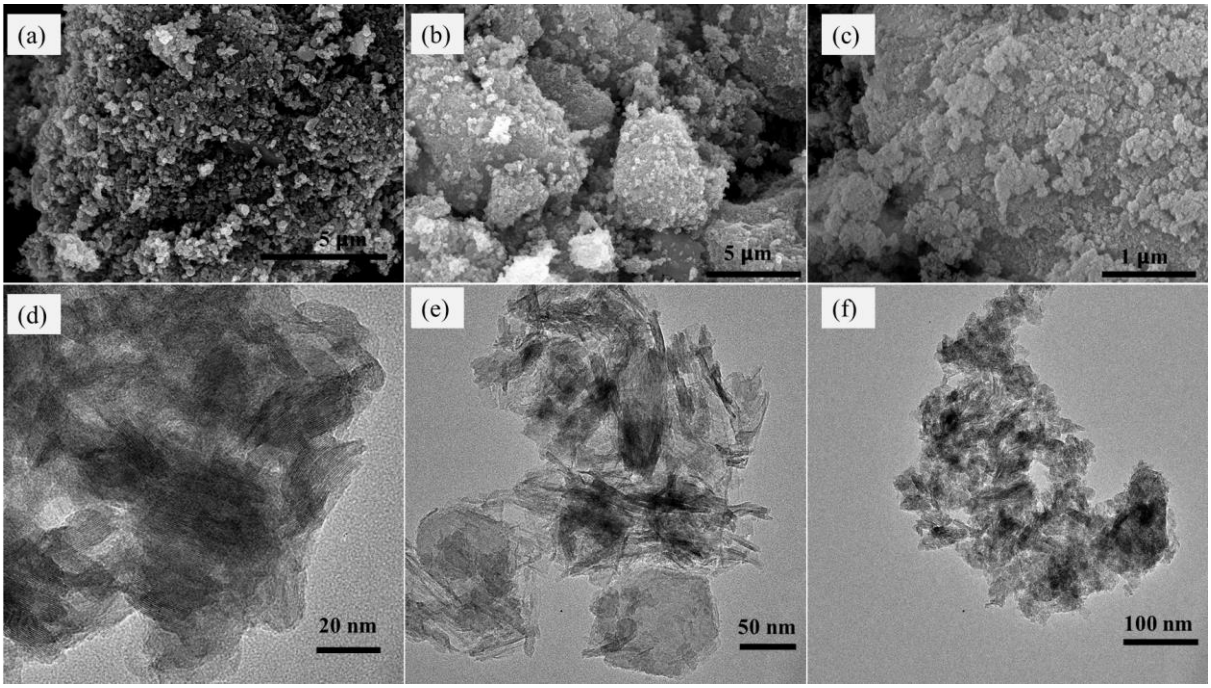

Figure 3. Scanning electron microscopic image of the samples in a-c (a-M200, b-M450 and c-M600) and Transmission electron microscopic images of the samples displayed in d-f (d-M200, e-M450 and f-M600) images.

3. The catalytic CO_2 hydrogenation reaction

Manganese-oxides prepared with different milling speed as well as several Pt and Cu-doped manganese-oxide were tested in CO_2 hydrogenation to form carbon-monoxide and methane at 573-823 K in a fixed bed flow catalytic reactor at ambient pressure. The summarized catalytic activity results, demonstrated by consumption rates and selectivities are discussed in the following chapters.

3.1 Effect of milling speed

All the ball-milled manganese-oxide prepared with different milling speed (M200, M450, M600) were active in CO_2 hydrogenation reaction at > 600 K and was producing mostly carbon-monoxide and some methane (**Fig 4a**). In the case of the reaction tested at 873 K, M600 catalysts showed the highest CO_2 consumption rate (~20.000 nmol*g^{-1}*s^{-1}) followed by M450 (17.500 nmol*g^{-1}*s^{-1}). Both M600 and M450 were almost 2 times more active compared to the catalyst milled at 200 rpm (~10.000 nmol*g^{-1}*s^{-1}). The high activity of manganese-oxide milled at higher speeds can be attributed to the high specific surface area and special porosity as well as the morphological differences. Furthermore, the samples milled with different speed after the pretreatment in hydrogen showed diversity in the ratio of Mn^{4+}: Mn^{3+}: Mn^{2+} (**Fig S7 a**), which can affect the catalytic activity. After the pretreatment, the birnessite type σ-MnO_2 ratio was decreased and mostly amorphous or nanoscaled $Mn(II, III)_3O_4$ and Mn(II)O was presented in the catalyst before the reaction.

It is interesting to note, that these kinds of noble metal-free oxides have striking activity compared to mesoporous MnO_2 samples and also is competitive with others (e.g. Ni, Co)-based oxides in CO_2 activation[14]. All M200, M450 and M600 was stable at 873 K under reaction condition for ~10 hrs (**Fig 4b**).

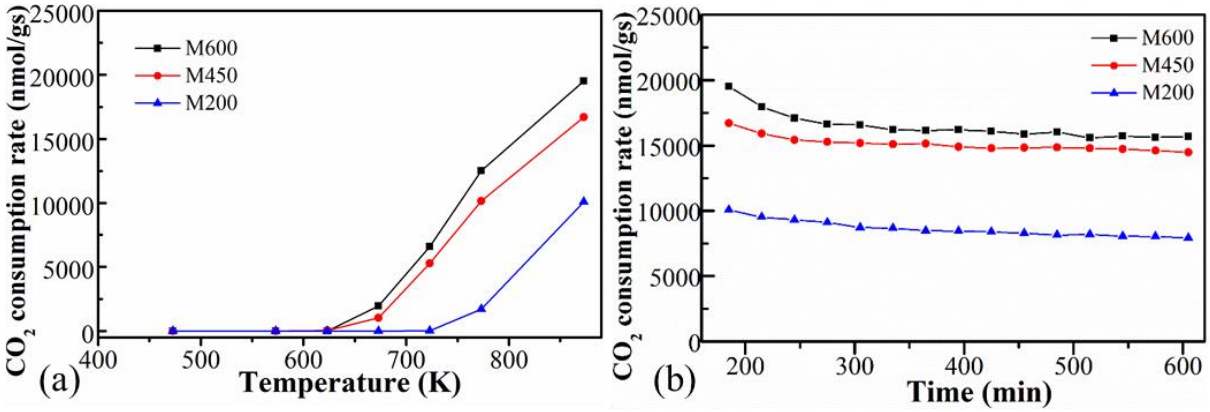

Figure 4. The CO_2 consumption rate of the manganese oxides synthesized by different milling speed (200 rpm-M200, 450 rpm-M450 and 600 rpm-M600) as a function of temperature (a) and function of time (b).

3.2 Effect of one-pot loading of Pt and Cu doped catalysts

To enhance the catalytic activity, a simple one-pot method was used to dope 3 wt% of Pt and Cu into the manganese-oxide nanoflakes during the milling process. The catalytic activity was significantly enhanced by adding Pt into the manganese-oxide structure at 673 K (**Fig 5a.**). In the case of the Pt-doped manganese-oxide catalyst milled under different speed, ~12-13 times increment in catalytic activity was observed, showing the presence of the significant role of the Pt where the effect of the milling speed was insignificant. Cu-doping resulted in a 2-3 times increment in catalytic activity compared to the pure manganese-oxide catalysts.

At higher temperature (873 K) displayed in **Fig.5b**, the catalytic boosting effect of Pt, as well as Cu-doping, was negligible. All the metal-loaded catalysts showed similarly high activity (~20.000 nmol*g^{-1}*s^{-1}) as the pure manganese-oxide milled at 600rpm. This phenomenon shows that the special mixed Mn(IV, III, II)-oxide role is crucial in the catalytic activity at a higher temperature. These changes illustrate that temperature plays an important role in the manganese oxide-based catalyst due to crystal structure changes and reducibility of the manganese oxides.

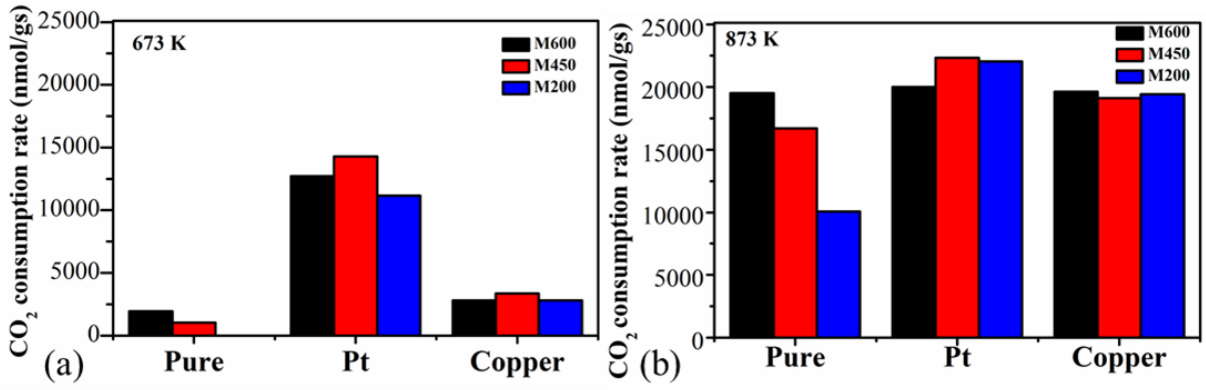

Figure 5. Temperature effect for the CO_2 consumption rate of the samples at (a) 673 K and (b) 873 K.

3.3 Effect of Platinum incorporation (milling vs. impregnation)

3 different types of Pt-loaded M600 were prepared by using the one-pot synthesis, incipient wetness impregnation as well as loading of pre-synthesized 5 nm Pt nanoparticles to the catalysts. All Pt-doped catalysts displayed almost the same catalytic activity (**Fig 6a-b.**). Usually, wet impregnation method or even designed surfaces by adding controlled sized nanoparticles resulted in specific loading of the metal onto the surface as well as a catalytic activity increment[39]. These tests support the idea that the main working surface of these kinds of catalysts is based on the manganese-oxide, regardless of the quality and type of doped metal onto the surface.

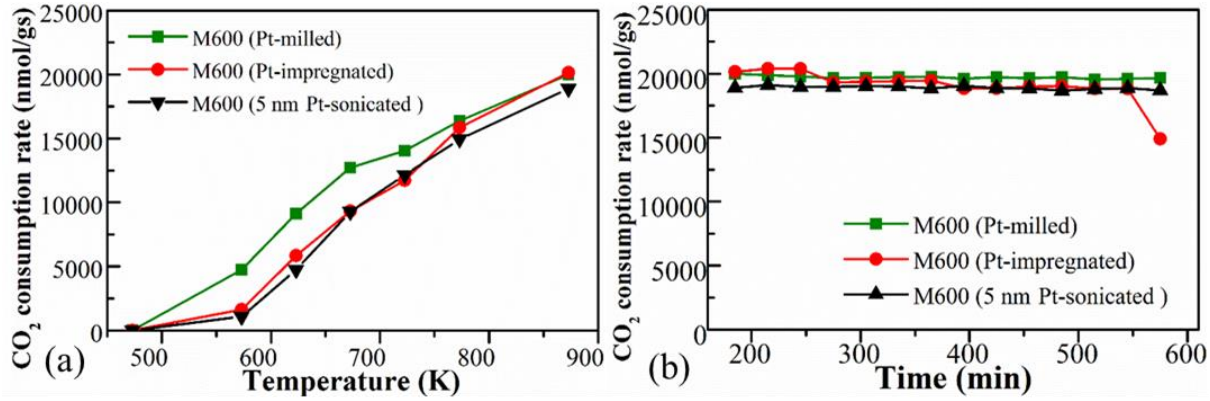

Figure 6. The CO_2 consumption rate of the Pt-doped M600 manganese-oxide prepared by the one-pot method, incipient wetness impregnation method as well as designed incorporation of controlled-sized 5 nm Pt nanoparticles as a function of temperature (a) and function of time (b).

3.4 Selectivity towards methane

In the case of the selectivity, these catalysts mostly produced carbon-monoxide (> 95 %) and a smaller amount of methane. Most catalysts started to produce methane with a small ratio at elevated temperature (~623 K) and after a short increment shifting of the products into the formation of carbon-monoxide was observed (**Fig 7a**) as expected from the thermodynamics of the CO_2 hydrogenation reaction in the gas phase[14]. In the case of the Pt/M600 catalysts produced by the one-

pot milling process, methane formation was significant compared to pure and Cu-loaded catalysts prepared by using different milling speed. This shows that, however, the catalytic activity is not highly influenced by the metal-loading, the Pt/MnO_x interphase is crucial in the methane selectivity. The Pt-loaded manganese-oxide prepared by the one-pot synthesis has 1.5-2 times higher selectivity towards methane compared to the Pt-loaded MnOx catalyst synthesized by the wet impregnation or the designing process showing the influence of the formed Pt/MnOx during the reaction (**Fig 7b**).

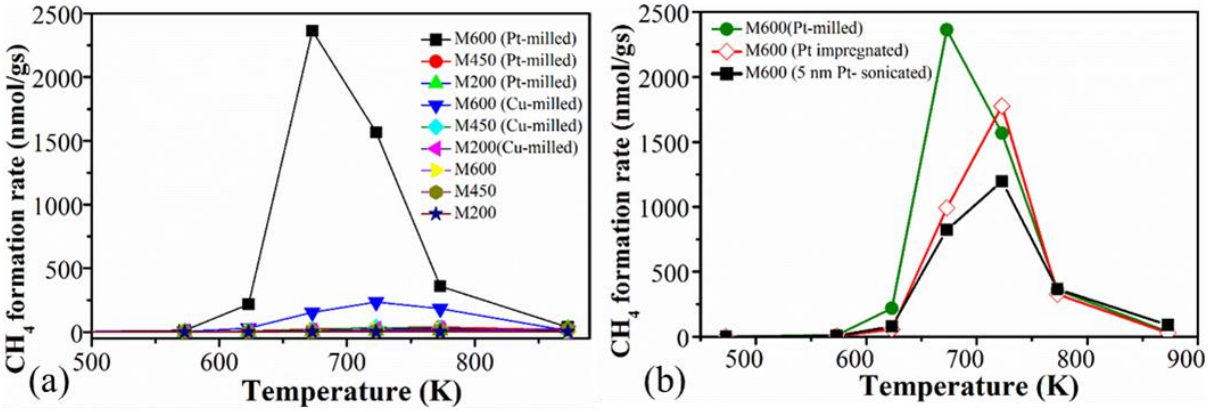

Figure 7. The formation rate of methane during CO_2 hydrogenation reaction in the case of (a) pure, Pt-loaded and Cu-loaded catalysts prepared by using different milling speed and (b) M600 doped with Pt by a different method.

4 Conclusion

A novel, mechanochemical synthesis, which can be easily used in scaled-up synthetic industries were successfully used to prepare manganese oxide nanoflakes and nanorods. The shape, porosity, specific surface area, as well as the ratio of the different oxidation states of the Mn-ion in the structure, can be tuned by the milling speed. Pt-loaded and Cu-loaded MnOx structures were prepared with the same one-pot technique and all the samples were tested in CO_2 hydrogenation reaction in the gas phase.

Pure MnOx milled at 600 rpm speed showed the highest catalytic activity where Pt-loading, as well as Cu-loading, was insignificant at higher temperatures. The presence of the different oxidation states of the manganese in the structure plays an important role in the CO_2 activation process. However, Pt-loading can improve methane selectivity. The one-pot synthesized Pt-loaded MnOx nanostructure showed the highest methane selectivity compared to the Pt-loaded MnOx catalyst synthesized by the wet impregnation or the designing process using controlled sized Pt nanoparticles showing the high impact of the formed Pt/MnOx interface on the selectivity of the catalytic CO_2 hydrogenation reaction.

5 Acknowledgement

This paper was supported by the Hungarian Research Development and Innovation Office through grants NKFIH OTKA PD 120877 of AS. ÁK, and KZ is grateful for the fund of NKFIH (OTKA) K112531 & NN110676 and K120115, respectively. The financial support of the Hungarian National Research, Development and Innovation Office through the GINOP-2.3.2-15-2016-00013 project "Intelligent materials based on functional surfaces - from syntheses to applications" and the Ministry of Human Capacities through the EFOP-3.6.1-16-2016-00014 project and the 20391-3/2018/FEKUSTRAT are acknowledged.

Materials and methods

Chemicals

Manganese (II) chloride tetrahydrate ($MnCl_2*4H_2O$), potassium permanganate ($KMnO_4$), platinum(IV) chloride ($H_2PtCl_6xH_2O$), copper (II) chloride ($CuCl_2$), sodium hydroxide (NaOH), platinum (II) acetylacetonate ($C_{10}H_{16}O_4Pt$), polyvinylpyrrolidone (PVP, MW= 40,000) and ethylene-glycol $(CH_2OH)_2$ were purchased from Sigma Aldrich. All chemicals and reagents used in this study were at least in analytical grade and used without further purification. Ultrapure water was used for all synthesis and washing.

Synthesis of manganese oxides (milling)

Mixed the manganese (II) chloride dihydrate and potassium permanganate with 0.5 molar ratio and added 0.09 M sodium hydroxide and 5 ml of water into the milling system. In further, precursor materials milled at 200 rpm, 450 rpm and 600 rpm speed, respectively for 4 hours in milling machine the Planetary Mono Mill Pulverisette 6 (Fritsch GmbH, Germany). The final product was obtained after the filtration, washing with water and freeze-drying overnight. The final products named M200, M450 and M600, respectively.

Synthesis of Pt and Cu-doped manganese oxides (used milling)

In case of platinum and copper doping, 0.0005 M platinum (IV) chloride and 0.0005 M copper (II) chloride added to the milling chamber with at the beginning with precursors as the amount used for pure samples and used corresponding 3 different milling speeds 200rpm, 450rpm and 600rpm for 4 hours, respectively. The final product was obtained after the filtration, washing with water and freeze-drying overnight.

Synthesis of platinum nanoparticles doped manganese oxides

Firstly, 5 nm Pt nanoparticles with controlled size were produced[40]. Here, 0.04 g Platinum (II) acetylacetonate and 0.035 g polyvinylpyrrolidone (PVP, MW = 40,000) was dissolved in 5 ml ethylene-glycol and ultrasonicated for 30 minutes to get a homogenous solution. The reactor is a three-necked round bottom flask, which is evacuated and purged with atmospheric pressure argon gas for several cycles to get rid of additional oxygen and water. After three purging cycles, the flask was immersed in an oil bath heated to 473 K under vigorous stirring of the reaction mixture as well as the oil bath. After 10 minutes of reaction, the flask was cooled down to room temperature. The suspension is precipitated with adding acetone and centrifuging. The nanoparticles are washed by centrifuging with hexane and redispersing in ethanol for at least 2-3 cycles and finally redispersed in ethanol.

To fabricate supported catalysts, the ethanol suspension of 5 nm Pt nanoparticles to reach a loading of 3 wt % and the manganese oxide support ball-milled at 600 rpm were mixed together in ethanol and sonicated in an ultrasonic bath (40 kHz, 80 W) for 3 hours[14]. The supported nanoparticles were collected by centrifugation. The products were washed with ethanol three times before they were dried at 353 K overnight. The required amount of Pt nanoparticle suspension was calculated based on ICP measurements.

Synthesis of platinum nanoparticles doped manganese oxides (with wet incipient wetness impregnation method)

In this case, the required amount of $H_2PtCl_6.xH_2O$ (to reach 3 wt% of metallic Pt) was dissolved into a determined amount of ethanol. The ethanolic solution than was filtrated into the pores of the manganese oxide support ball-milled at 600rpm. The supported

catalyst was dried and calcined before the catalytic reaction to decompose the Pt-salt and to reach metallic Pt form.

Catalytic CO_2 activation reaction over manganese-oxide catalysts

Pretreatment:

Before the catalytic experiments, the as-received catalysts were oxidized in O_2 atmosphere at 300 °C for 30 min to remove the surface contaminants, as well as the PVP capping agent and thereafter, were reduced in H_2 at 300 °C for 60 min.

Hydrogenation of carbon dioxide in a continuous flow reactor:

Catalytic reactions were carried out at atmospheric pressure in a fixed-bed continuous-flow reactor (200 mm long with 8 mm i.d.) which was heated externally[41]. The dead volume of the reactor was filled with quartz beads. The operating temperature was controlled by a thermocouple placed inside the oven close to the reactor wall, to assure precise temperature measurement. For catalytic studies, small fragments (about 1 mm) of slightly compressed pellets were used. Typically, the reactor filling contained 150 mg of catalyst. In the reacting gas mixture, the CO_2: H_2 molar ratio was 1:4, if not denoted otherwise. The CO_2: H_2 mixture was fed with the help of mass flow controllers (Aalborg), the total flow rate was 50 ml/min. The reacting gas mixture flow entered and left the reactor through an externally heated tube in order to avoid condensation. The analysis of the products and reactants was performed with an Agilent 6890 N gas chromatography using HP-PLOTQ column. The gases were detected simultaneously by thermal conductivity (TC) and flame ionization (FI) detectors. The CO_2 was transformed by a methanizer to methane and it was also analyzed by FID.

Characterization of the samples

All the samples were characterized with a Rigaku Miniflex II powder X-ray diffractometer using a Cu Kα radiation source (λ = 0.15418 nm) operating at 30 kV and 15 mA at room temperature and a scanning rate of 0.5 degrees min^{-1} in the 10–65° 2θ range was used. High-resolution transmission electron microscopy HR-TEM (FEI TECNAI G2 20 X-TWIN) operated at 200 kV accelerating voltage used to study the morphology of particles and crystal structure determination. The morphological image and the chemical composition of the samples measured by the scanning electron microscopy and the samples were mounted on a sample holder with carbon glue. Energy-dispersive X-ray spectroscopy (EDS) and high-resolution secondary electron (SE) images were taken by a Hitachi S-4700 Type II instrument (30 kV accelerating voltage). The thermal behaviour of samples was investigated using a Thermogravimetry (TA Instruments Q500 TGA). The instrument worked at 750 °C under a constant flow of air and nitrogen, and the heating rate was 5 °C/min. The samples, between 10–20 mg, were placed into high-purity alpha platinum crucibles. Differential scanning calorimetric analysis prevailed by Q20 (TA Instruments) at 600 °C under constant airflow and the heating-cooling rate was 5 °C/min. The Raman spectra were collected using a SENTERRA Raman microscope (Bruker Optics, Inc.) at 532 nm with a 1s integration (with 3 reputations) at a resolution of 4 cm^{-1} and interferometer resolution 0.5 cm^{-1}. The Brunauer-Emmett-Teller (BET) surface area and pore radius were measured with 3H-2000 BET-A surface area analyzer.

6 References

(1) Lewis, N. S.; Nocera, D. G. Powering the Planet: Chemical Challenges in Solar Energy Utilization. *Proc. Natl. Acad. Sci.* **2006**, *103* (43), 15729–15735. https://doi.org/10.1073/pnas.0603395103.

(2) Bratt, D. Catalytic CO2 Hydrogenation - Literature Review : Technology Development since 2014. **2016**.

(3) Yang, H.; Zhang, C.; Gao, P.; Wang, H.; Li, X.; Zhong, L.; Wei, W.; Sun, Y. A Review of the Catalytic Hydrogenation of Carbon Dioxide into Value-Added Hydrocarbons. *Catal. Sci. Technol.* **2017**, *7* (20), 4580–4598. https://doi.org/10.1039/c7cy01403a.

(4) Lee, S.; Xu, H. XRD and Tem Studies on Nanophase Manganese Oxides in Freshwater Ferromanganese Nodules from Green Bay, Lake Michigan. *Clays Clay Miner.* **2016**, *64* (5), 523–536. https://doi.org/10.1346/CCMN.2016.064032.

(5) Post, J. E. Manganese Oxide Minerals : Crystal Structures and Economic And. *Proc Natl Acad Sci USA* **1999**, *96* (March), 3447–3454.

(6) Chen, P. Manganese Metabolism in Humans. *Front. Biosci.* **2018**, *23* (9), 4665. https://doi.org/10.2741/4665.

(7) Huang, X.; Chen, T.; Zou, X.; Zhu, M.; Chen, D.; Pan, M. The Adsorption of Cd(II) on Manganese Oxide Investigated by Batch and Modeling Techniques. *Int. J. Environ. Res. Public Health* **2017**, *14* (10). https://doi.org/10.3390/ijerph14101145.

(8) Xin Zhang, Y.; Long Guo, X.; Huang, M.; Dong Hao, X.; Yuan, Y.; Hua, C. Engineering Birnessite-Type MnO2nanosheets on Fiberglass for PH-Dependent Degradation of Methylene Blue. *J. Phys. Chem. Solids* **2015**, *83*, 40–46. https://doi.org/10.1016/j.jpcs.2015.03.015.

(9) Gorlin, Y.; Lassalle-Kaiser, B.; Benck, J. D.; Gul, S.; Webb, S. M.; Yachandra, V. K.; Yano, J.; Jaramillo, T. F. In Situ X-Ray Absorption Spectroscopy Investigation of a Bifunctional Manganese Oxide Catalyst with High Activity for Electrochemical Water Oxidation and Oxygen Reduction. *J. Am. Chem. Soc.* **2013**, *135* (23), 8525. https://doi.org/10.1021/ja3104632.

(10) Thenuwara, A. C.; Shumlas, S. L.; Attanayake, N. H.; Cerkez, E. B.; McKendry, I. G.; Frazer, L.; Borguet, E.; Kang, Q.; Zdilla, M. J.; Sun, J.; et al. Copper-Intercalated Birnessite as a Water Oxidation Catalyst. *Langmuir* **2015**, *31* (46), 12807–12813. https://doi.org/10.1021/acs.langmuir.5b02936.

(11) Wang, W.; Shao, Z.; Liu, Y.; Wang, G. Removal of Multi-Heavy Metals Using Biogenic Manganese Oxides Generated by a Deep-Sea Sedimentary Bacterium - Brachybacterium Sp. Strain Mn32. *Microbiology* **2009**, *155* (6), 1989–1996. https://doi.org/10.1099/mic.0.024141-0.

(12) Guan, H.; Dang, W.; Chen, G.; Dong, C.; Wang, Y. RGO/KMn8O16composite as Supercapacitor Electrode with High Specific Capacitance. *Ceram. Int.* **2016**, *42* (4), 5195–5202. https://doi.org/10.1016/j.ceramint.2015.12.043.

(13) Atwater, T. B.; Salkind, A. J. Lithium Potassium Manganese Mixed Metal Oxide Material for Rechargeable Electrochemical Cells. **2010**, 4–8.

(14) Sápi, A.; Rajkumar, T.; Ábel, M.; Efremova, A.; Grósz, A.; Gyuris, A.; Ábrahámné, K. B.; Szenti, I.; Kiss, J.; Varga, T.; et al. Noble-Metal-Free and Pt Nanoparticles-Loaded, Mesoporous Oxides as Efficient Catalysts for CO2 Hydrogenation and Dry Reforming with Methane. *J. CO2 Util.* **2019**, *32* (April), 106–118. https://doi.org/10.1016/j.jcou.2019.04.004.

(15) Prasad Yadav, T.; Manohar Yadav, R.; Pratap Singh, D. Mechanical Milling: A Top Down Approach for the Synthesis of Nanomaterials and Nanocomposites. *Nanosci. Nanotechnol.* **2012**, *2* (3), 22–48. https://doi.org/10.5923/j.nn.20120203.01.

(16) Gagrani, A.; Zhou, J.; Tsuzuki, T. Solvent Free Mechanochemical Synthesis of MnO2for the Efficient Degradation of Rhodamine-B. *Ceram. Int.* **2018**, *44* (5), 4694–4698. https://doi.org/10.1016/j.ceramint.2017.12.050.

(17) Liu, H.; Zhao, K. Asymmetric Flow Electrochemical Capacitor with High Energy Densities Based on Birnessite-Type Manganese Oxide Nanosheets and Activated Carbon Slurries. *J. Mater. Sci.* **2016**, *51* (20), 9306–9313. https://doi.org/10.1007/s10853-016-0177-0.

(18) Iyer, A.; Dutta, P.; Suib, S. Water Oxidation Catalysis Using Amorphous Manganese Oxides, Octahedral Molecular Sieves (OMS-2), and Octahedral Layered (OL-1) Manganese Oxide Structures - The Journal of Physical Chemistry C (ACS Publications). *J. Phys. Chem. C* **2012**, *116*, 6474–6483.

(19) Anandan, S.; Gnana Sundara Raj, B.; Lee, G. J.; Wu, J. J. Sonochemical Synthesis of Manganese (II) Hydroxide for Supercapacitor Applications. *Mater. Res. Bull.* **2013**, *48* (9), 3357–3361. https://doi.org/10.1016/j.materresbull.2013.05.021.

(20) Qian, S.; Cheney, M. A.; Jose, R.; Banerjee, A.; Bhowmik, P. K.; Okoh, J. M. Synthesis and Characterization of Birnessite and Cryptomelane Nanostructures in Presence of Hoffmeister Anions. *J. Nanomater.* **2009**, *2009*. https://doi.org/10.1155/2009/940462.

(21) Zhu, J.; He, J. Facile Synthesis of Graphene-Wrapped Honeycomb MnO 2 Nanospheres and Their Application in Supercapacitors. *ACS Appl. Mater. Interfaces* **2012**, *4* (3), 1770–1776. https://doi.org/10.1021/am3000165.

(22) Yan, J.; Fan, Z.; Wei, T.; Qian, W.; Zhang, M.; Wei, F. Fast and Reversible Surface Redox Reaction of Graphene-MnO2 Composites as Supercapacitor Electrodes. *Carbon N. Y.* **2010**, *48* (13), 3825–3833. https://doi.org/10.1016/j.carbon.2010.06.047.

(23) Aghazadeh, M.; Bahrami-Samani, A.; Gharailou, D.; Maragheh, M. G.; Ganjali, M. R.; Norouzi, P. Mn3O4 Nanorods with Secondary Plate-like Nanostructures; Preparation, Characterization and Application as High Performance Electrode Material in Supercapacitors. *J. Mater. Sci. Mater. Electron.* **2016**, *27* (11), 11192–11200. https://doi.org/10.1007/s10854-016-5239-1.

(24) Fang, M.; Tan, X.; Liu, M.; Kang, S.; Hu, X.; Zhang, L. Low-Temperature Synthesis of Mn 3O 4 Hollow-Tetrakaidecahedrons and Their Application in Electrochemical Capacitors. *CrystEngComm* **2011**, *13* (15), 4915–4920. https://doi.org/10.1039/c1ce05337j.

(25) Julien, C.; Massot, M.; Baddour-Hadjean, R.; Franger, S.; Bach, S.; Pereira-Ramos, J. P. Raman Spectra of Birnessite Manganese Dioxides. *Solid State Ionics* **2003**, *159* (3–4), 345–356. https://doi.org/10.1016/S0167-2738(03)00035-3.

(26) Julien, C. M.; Massot, M.; Poinsignon, C. Lattice Vibrations of Manganese Oxides: Part I. Periodic Structures. *Spectrochim. Acta - Part A Mol. Biomol. Spectrosc.* **2004**, *60* (3), 689–700. https://doi.org/10.1016/S1386-1425(03)00279-8.

(27) Fujiwara, K.; Akedo, K.; Tasaki, Y.; Nakatsuka, A.; Nakayama, N. Structure and Thermal Decomposition of KxMnO2・yH2O Prepared by Sol-Gel Method. *Trans. Mater. Res. Soc. Japan* **2014**, *34* (3), 447–450. https://doi.org/10.14723/tmrsj.34.447.

(28) Wang, G.; Shao, G.; Du, J.; Zhang, Y.; Ma, Z. Effect of Doping Cobalt on the Micro-Morphology and Electrochemical Properties of Birnessite MnO2. *Mater. Chem. Phys.* **2013**, *138* (1), 108–113. https://doi.org/10.1016/j.matchemphys.2012.11.024.

(29) Liu, H.; Zhang, H.; Shi, L.; Hai, X.; Ye, J. Lattice Oxygen Assisted Room-Temperature Catalytic Process: Secondary Alcohol Dehydrogenation over Au/Birnessite Photocatalyst. *Appl. Catal. A Gen.* **2016**, *521*, 149–153. https://doi.org/10.1016/j.apcata.2015.10.027.

(30) Chakrabarti, S.; Dutta, B. K.; Apak, R. Active Manganese Oxide: A Novel Adsorbent for Treatment of Wastewater Containing Azo Dye. *Water Sci. Technol.* **2009**, *60* (12), 3017–3024. https://doi.org/10.2166/wst.2009.758.

(31) Cheney, M. A.; Bhowmik, P. K.; Qian, S.; Joo, S. W.; Hou, W.; Okoh, J. M. A New Method

of Synthesizing Black Birnessite Nanoparticles: From Brown to Black Birnessite with Nanostructures. *J. Nanomater.* **2008**, *2008* (1), 1–8. https://doi.org/10.1155/2008/763706.

(32) Feng, Q.; Yanagisawa, K.; Yamasaki, N. Synthesis of Birnessite-Type Potassium Manganese Oxide. *J. Mater. Sci. Lett.* **1997**, *6* (3), 5–7. https://doi.org/10.1023/A:1018577523676.

(33) Zaitsev, A. I.; Zemchenko, M. A.; Mogutnov, B. M. Thermodynamic Properties of Manganese Silicides. *Zh. Fiz. Khim.* 1989, pp 1451–1458.

(34) El-Sawy, A. M.; King'ondu, C. K.; Kuo, C.-H.; Kriz, D. A.; Guild, C. J.; Meng, Y.; Frueh, S. J.; Dharmarathna, S.; Ehrlich, S. N.; Suib, S. L. X-Ray Absorption Spectroscopic Study of a Highly Thermally Stable Manganese Oxide Octahedral Molecular Sieve (OMS-2) with High Oxygen Reduction Reaction Activity. *Chem. Mater.* **2014**, *26* (19), 5752–5760. https://doi.org/10.1021/cm5028783.

(35) Jacob, K. T.; Kumar, A.; Rajitha, G.; Waseda, Y. Thermodynamic Data for Mn 3O 4, Mn 2O 3 and MnO 2. *High Temp. Mater. Process.* **2011**, *30* (4), 459–472. https://doi.org/10.1515/HTMP.2011.069.

(36) Hernández, W. Y.; Centeno, M. A.; Ivanova, S.; Eloy, P.; Gaigneaux, E. M.; Odriozola, J. A. Cu-Modified Cryptomelane Oxide as Active Catalyst for CO Oxidation Reactions. *Appl. Catal. B Environ.* **2012**, *123–124*, 27–35. https://doi.org/10.1016/j.apcatb.2012.04.024.

(37) González, C.; Gutiérrez, J. I.; González-Velasco, J. R.; Cid, A.; Arranz, A.; Arranz, J. F. Application of Differential Scanning Calorimetry to the Reduction of Several Manganese Oxides. *Journal of Thermal Analysis and Calorimetry*. 1998, pp 985–989. https://doi.org/10.1023/A:1010132606114.

(38) Xue, Q.; Zhang, Q. Agar Hydrogel Template Synthesis of Mn 3 o 4 Nanoparticles through an Ion Diffusion Method Controlled by Ion Exchange Membrane and Electrochemical Performance. *Nanomaterials* **2019**, *9* (4). https://doi.org/10.3390/nano9040503.

(39) Sápi, A.; Halasi, G.; Grósz, A.; Kiss, J.; Kéri, A.; Ballai, G.; Galbács, G.; Kukovecz, Á.; Kónya, Z. Designed Pt Promoted 3D Mesoporous Co3O4 Catalyst in CO2 Hydrogenation. *J. Nanosci. Nanotechnol.* **2018**, *19* (1), 436–441. https://doi.org/10.1166/jnn.2019.15779.

(40) Sápi, A.; Dobó, D. G.; Sebok, D.; Halasi, G.; Juhász, K. L.; Szamosvölgyi, A.; Pusztai, P.; Varga, E.; Kálomista, I.; Galbács, G.; et al. Silica Based Catalyst Supports Are Inert, Aren't They? – Striking Differences in Ethanol Decomposition Reaction Originated from Meso-& Surface Fine Structure Evidenced by Small Angle X-Ray Scattering. *J. Phys. Chem. C* **2017**, *121* (9), 5130–5136. https://doi.org/10.1021/acs.jpcc.7b00034.

(41) Sápi, A.; Halasi, G.; Kiss, J.; Dobó, D. G.; Juhász, K. L.; Kolcsár, V. J.; Ferencz, Z.; Vári, G.; Matolin, V.; Erdöhelyi, A.; et al. In Situ DRIFTS and NAP-XPS Exploration of the Complexity of CO2 Hydrogenation over Size-Controlled Pt Nanoparticles Supported on Mesoporous NiO. *J. Phys. Chem. C* **2018**, *122* (10), 5553–5565. https://doi.org/10.1021/acs.jpcc.8b00061.